JOURNAL OF GEOPHYSICAL RESEARCH, VOL. 113, B09404, doi:10.1029/2007JB005414, 2008

Crustal deformation and block kinematics in transition from collision to subduction: Global positioning system measurements in northern Taiwan, 1995–2005

Ruey-Juin Rau,[1,2] Kuo-En Ching,[1] Jyr-Ching Hu,[3] and Jian-Cheng Lee[4]

Received 1 October 2007; revised 1 June 2008; accepted 26 June 2008; published 9 September 2008.

[1] We present global positioning system (GPS) measurements for the period 1995–2005 at 125 campaign-surveyed sites in northern Taiwan. Based on elastic, rotating block modeling analyses derived from the GPS data, we describe the transitional tectonics from arc–continent (Luzon–Chinese) collision to the converging Ryukyu trench subduction and back-arc opening along the Chinese continental margin. Station velocities relative to station S01R, in the Chinese stable continental margin, were estimated from coordinate time series of each station by using the weighted least squares technique. We found two distinct deformation patterns in two geological areas, which are basically separated by the surface projection of the NW-trending boundary of the subducting Philippine Sea plate across northern Taiwan: (1) a waning collision area to the west and (2) a transition zone to the east. In the waning collision area, the horizontal velocity field shows vectors of 0.3–7.3 mm/yr toward the NW in the foothills and the Hsuehshan Range of northwestern Taiwan. The tectonic blocks represent a significant NW–SE internal contraction along with a small block rotation rate (<3.0°/Myr). The transition zone can be further divided into an outer range and inner range with distinguishing rotation rates and deformation behaviors. In the outer range of the transition zone, velocities of 1.0–7.8 mm/yr from south to north rotating from 008° to 143° is found in the northernmost foothills and the Hsuehshan Range. The tectonic blocks within the outer range are characterized by a coherent rotation (low internal strain rate of <0.10 μstrain/yr) with an angular velocity of ~5.1°/Myr, where the Euler pole is located near its southeastern boundary. In the inner range of transition zone, a larger clockwise rotation from west to east, with horizontal velocities of 9.3–41.2 mm/yr from 053° to 146°, are found in the northernmost Central Range. The tectonic blocks of the inner range reveal a remarkable NW–SE internal extension with an ultrarapid clockwise rotation (~47.3°/Myr) where the Euler pole is near the southern boundary of the range close to the collision corner with the colliding Luzon arc. The trench roll-back together with back-arc opening are interpreted to be substantially superposed on the arc–continent collision-induced rotation in the transition zone with particular regard to the inner range of the northeast Taiwan mountain belt.

Citation: Rau, R.-J., K.-E. Ching, J.-C. Hu, and J.-C. Lee (2008), Crustal deformation and block kinematics in transition from collision to subduction: Global positioning system measurements in northern Taiwan, 1995–2005, *J. Geophys. Res.*, *113*, B09404, doi:10.1029/2007JB005414.

1. Introduction

[2] The Taiwan orogen is a product of the Plio-Pleistocene oblique collision between the north–south trending Luzon island arc of the Philippine Sea plate and the northeast–southwest trending Chinese continental margin of the Eurasian plate (Figure 1) [*Suppe*, 1984; *Ho*, 1988; *Huang et al.*, 2006]. East and northeast of Taiwan, a subduction polarity reversal occurs as the Philippine Sea plate switches from an overriding plate above the east-dipping South China slab to a northward subducting plate under the Ryukyu arc and the Eurasian continental margin. The boundary of the polarity reversal is likely located along the western edge of the subducting slab of the Philippine Sea plate in northern Taiwan [*Teng et al.*, 1992]. First initiated by a subduction reversal and subsequent southward propagation of the collision zone, northern Taiwan no longer experiences collisions and is now moving into the regime of Ryukyu trench [*Suppe*, 1984; *Viallon et al.*, 1986; *Teng*, 1996; *Clift et al.*, 2003].

[1]Department of Earth Sciences, National Cheng Kung University, Tainan, Taiwan.
[2]Earth Dynamic System Research Center, National Cheng Kung University, Tainan, Taiwan.
[3]Department of Geosciences, National Taiwan University, Taipei, Taiwan.
[4]Institute of Earth Sciences, Academia Sinica, Taipei, Taiwan.

0148-0227/08/2007JB005414$09.00

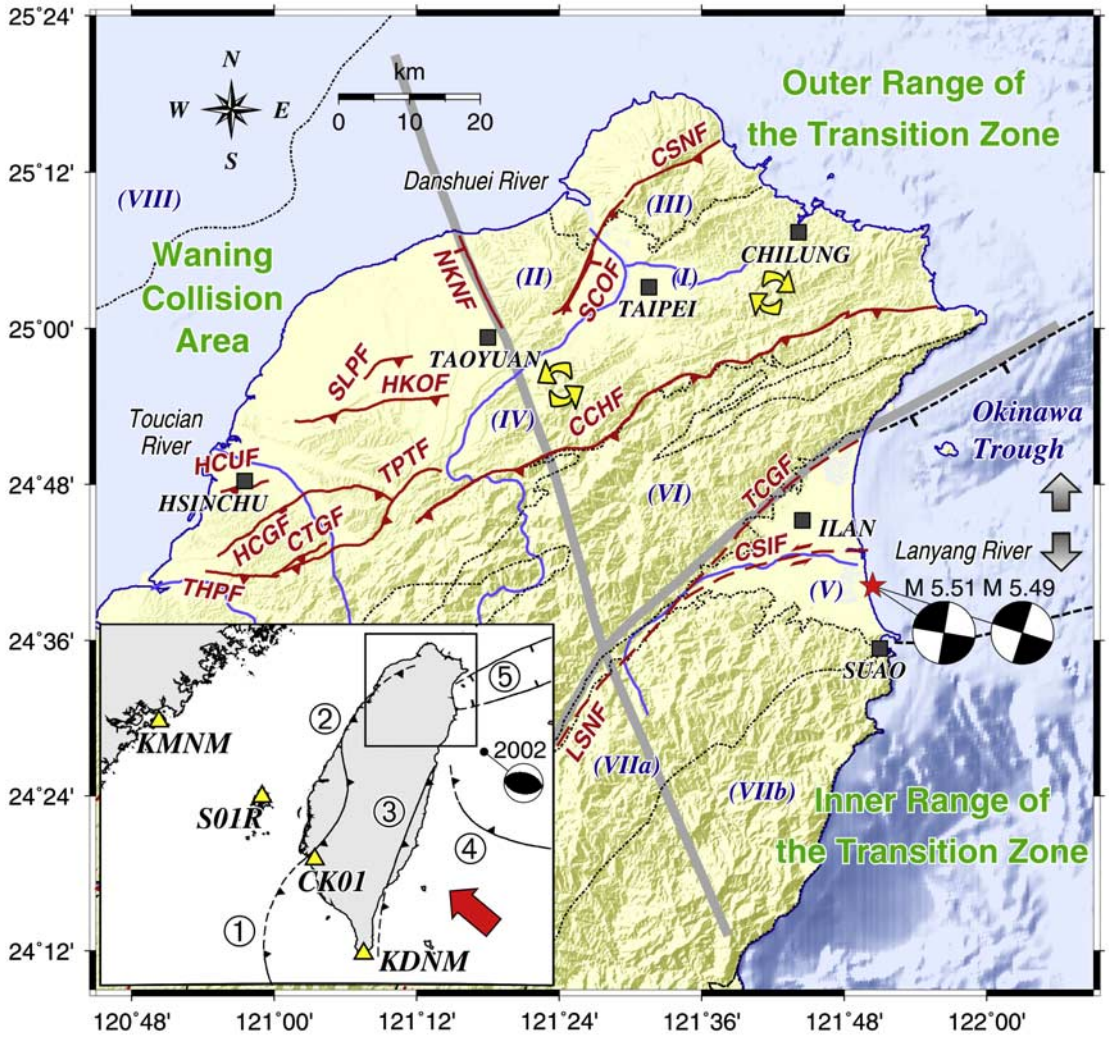

Figure 1. The regional tectonic setting of northern Taiwan. Solid squares denote the locations of cities. Red lines indicate major faults and blue lines major rivers. Shaded lines bound the waning collision area, the outer range of transition zone, and the inner range of transition zone. I–VIII: I, Taipei Basin; II, Linkou tableland; III, Tatun volcanic edifice; IV, Western Foothills; V, Ilan plain; VI, Hsueshan Range; VIIa, Backbone Range; VIIb, Metamorphic Complex; VIII, Kuanyin basement high. CSNF, Chinshan fault; SCOF, Shanchiao fault; NKNF, Nankan fault; SLPF, Shuanglianpo fault; HKOF, Hukou fault; TPTF, Tapingti fault; HCUF, Hsinchu fault; HCGF, Hsincheng fault; CTGF, Chutung fault; THPF, Touhuanping fault; CCHF, Chuchih fault; LSNF, Lishan fault; CSIF, Choshui fault; TCGF, Toucheng fault. Beach balls show the focal mechanism solutions for the M_w = 5.5 earthquakes. The yellow arrows denote the rotation directions [*Lu et al.*, 1995]. The motion of each fault is referred to the work of *Lu et al.* [1995]. The insert shows the geotectonic framework and major structural units of Taiwan between the Eurasian plate and Philippine Sea plate. Yellow triangles indicate the locations of the constrained local permanent GPS stations (section 3) used in this research. The red arrow represents the convergence direction of the Philippine plate. The beach ball in the insert is the focal mechanism solution for the 2002 M_L = 6.8 Hualien, Taiwan offshore earthquake. Numerals 1–5 indicate the Manila trench, the deformation front, the Longitudinal Valley fault, the Ryukyu trench, and the Okinawa trough, respectively.

Northern Taiwan now represents a postcollisional orogen which provides an opportunity to study crustal deformation in the transition from an arc–continent collision to subduction along a continental margin.

[3] One of the prominent tectonic features of the Taiwanese mountain belt is the major change in general structural trends in northeastern Taiwan (Figure 1). The mountain ranges in central and southern Taiwan trend NNE–SSW, whereas in northeastern Taiwan they trend ENE–WSW to E–W. This major change in structural trends occurs between 24°N and 25°N and has been interpreted to be the result of an interaction between the reversal of subduction

polarity at the plate corner and opening of the Okinawa trough [*Suppe*, 1984].

[4] The strata of northern Taiwan has experienced significant horizontal rotation and a transition from west to east as a result of contractions, block rotations, and transcurrent faulting; an extension has also taken place in northern Taiwan since the Plio-Pleistocene (Figure 1) [*Angelier et al.*, 1990; *Lu et al.*, 1995]. Paleomagnetic studies indicate a general counterclockwise rotation of $\sim 20^\circ$ in northwestern Taiwan since the middle to late Pliocene [*Lue et al.*, 1995]. By contrast, a clockwise rotation of $15-50^\circ$ has occurred in northeastern Taiwan during the same period [*Lee et al.*, 1991; *Lue et al.*, 1995] which was interpreted as in response to the oblique Taiwan arc–continent collision [*Angelier et al.*, 1986, 1990]. Geodetic and geological data indicate that the motion changes progressively from a shortening in northwestern Taiwan to an extension in the Ilan Plain in northeastern Taiwan; the southwestern extension of the Okinawa Trough [*Hu et al.*, 1996; *Teng and Lee*, 1996].

[5] A few earthquakes with $M \geq 5.5$ have occurred in northeastern Taiwan during the last decade wherein Figure 1 shows both P axes oriented from an E–W to NE–SW direction and T axes in N–S or NW–SE directions, both indicating an interaction between the extension from the opening of the Okinawa Trough and the compression from the oblique collision [*Kao et al.*, 1998]. Sandbox experiments and numerical modeling support geological and initial GPS observations in northern Taiwan [*Lu and Malavieille*, 1994; *Hu et al.*, 1996, 2002]; however, details of the deformation remain unclear. The purpose of this paper is to present our analysis of a decade's long, densely spaced campaign GPS data that describe current crustal deformation and constraints regarding the mechanisms of transition between an oblique collision and subduction processes in northern Taiwan.

2. Tectonic Settings of Northern Taiwan

[6] Northern Taiwan can be divided into three areas: a waning collision area (the Hsinchu area) to the southwest, an outer range of the transition zone (the Taipei area) to the north, and an inner range of the transition zone (the Ilan area) to the southeast (Figure 1). The waning collision area, comprising Quaternary tableland and the Tertiary Western Foothills, represents the northernmost part of active crustal shortening in Taiwan [*Angelier et al.*, 1986]. In general, NW–SE shortening, which is subparallel to the relative plate motion, is accommodated by several subparallel ENE–WSW trending reverse faults and folds. The outer range of the transition zone consists of two major physiographic/geological units: the Tertiary Western Foothills and Hsuehshan Range (Figure 1) [*Teng et al.*, 2001; *Shyu et al.*, 2005]. The major active structure in this area is the Shanchiao–Chinshan fault system, which is located along the frontal zone and marks the western margin of the Taipei basin. There is a vertical offset of strata of more than 700 m across the Shanchiao fault (SCOF) [*Wang et al.*, 1994, 1995; *Teng et al.*, 2001]. Structural analysis indicates that the Shanchiao fault appears to be an oblique–slip fault with both normal and strike–slip components [*Lee and Wang*, 1988; *Chu et al.*, 1998]. Shallow cores drilled in the Taipei basin suggest that at least three major events each with a slip of 1–3 m occurred in the past 11 Ka [*Huang et al.*, 2007]. This extension or transtension regime also occurs farther north along the Chinshan fault (CSNF) as evidence of an inversion from thrust to normal faulting from field observations in the Tatun volcano area [*Chan et al.*, 2006] and from reflection seismic profiles offshore [*Teng and Lee*, 1996; *Hsiao et al.*, 1999]. Therefore the Chinshan and Shanchiao faults seem to both be active in the same extensional or transtensional tectonic regime and jointly represent the active fault system west of the Taipei basin.

[7] Between the outer and inner ranges of the transition zones, the triangular Ilan plain is located at the western tip of the N–S opening Okinawa trough (Figure 1). The inner range of the transition zone is composed of the northern tip of the Eastern Central Range including the Backbone Range (Eocene to Miocene slates) and the Metamorphic Complex (Paleozoic to late Mesozoic greenschist-facies basement rocks). On the basis of geomorphologic investigations [*Shyu et al.*, 2005], two normal fault systems have been interpreted to bound the Ilan plain. Triangular facets, scarps and discontinuous faults along the northern flank of Ilan plain represent a zone of normal faults several km wide which has been named the Toucheng fault (TCGF) [*Lee*, 1991]. Fault traces are not well demonstrated by geomorphic features in the southern edge of the Ilan plain due to the sedimentary cover of alluvial fans of the Langyan River. In addition, a recent (March 2005) $M_w = 5.5$ earthquake doublet which occurred in the Ilan area indicates that the Lishan fault (LSNF), which separates the outer and inner ranges of the Taiwan mountain belt, might turn E–W and run across the middle of the plain to offshore. This is consistent with subsurface geological and geophysical surveys [*Jiang*, 1976] which mapped the boundary fault between the Hsuehshan and Backbone Ranges in the middle of the Ilan plain and identified the major fault as the Choshui fault (CSIF). The focal mechanisms of the 2005 earthquake doublet indicate left-lateral movement on the Choshui fault.

3. GPS Data Collection and Calculation

[8] A $\sim$10 km station-spacing GPS array in northern Taiwan (Figure 2) has been repeatedly surveyed by the Ministry of the Interior (MOI) since 1995. This array is composed of 120 campaign-surveyed stations. In this study, we also included five continuous stations (BANC, TAIW, TNML, TWTF, and YMSM) in northern Taiwan each of which was installed by various agencies, including the Central Weather Bureau (CWB), International GNSS Service (IGS), and MOI. During GPS campaign surveys in 1995–2005, about 86% (104 stations) of the 120 stations were occupied for 3–8 sessions and the other 14% (16 stations) were occupied for two sessions in 1995–2005 (Table 1). Every session was occupied 4–14 hours. The reasons why we did not abandon the 16 stations of observations with only two sessions in our solutions are because most of them have more than eight years of observations and some of them are located in critical locations.

[9] The campaign-surveyed and continuous GPS data were processed session by session with Bernese software

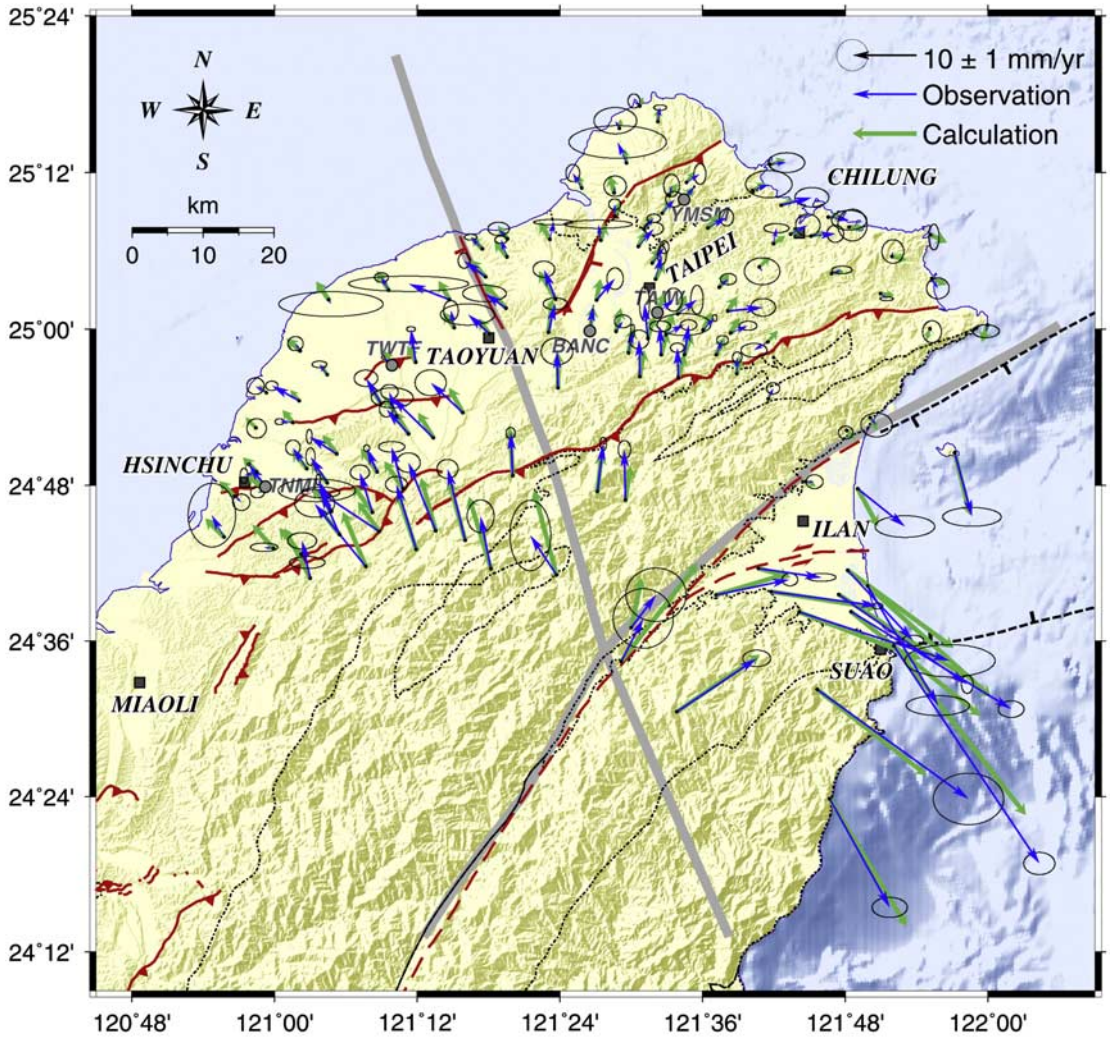

Figure 2. The GPS velocity field in northern Taiwan with respect to station S01R, the Penghu Island on the Chinese continental margin. The blue arrows indicate horizontal velocities. A 95% confidence error ellipse is shown at the tip of each velocity vector. The green arrows are shown as velocities derived from the optimal model. The small black dots are locations of the campaign-mode GPS stations. The large grey circles indicate the continuous GPS stations. Red lines denote major faults. Gray lines are the boundaries separating the waning collision area, the outer and inner ranges of the transition zone. Solid squares mark the locations of cities.

v.4.2 [*Hugentobler et al.*, 2001] to obtain the station coordinates. The precise ephemerides provided by IGS were employed and fixed during processing. To prevent unstable solutions of global IGS fiducial stations contaminating the estimates of campaign-surveyed data, the positions and velocities of four local permanent stations (CK01, S01R, KDNM, and KMNM; Figure 1) were determined from four global IGS fiducial stations (TSKB, GUAM, TID2 and WUHN) on the international terrestrial reference frame (ITRF2000) [*Altamimi et al.*, 2002] by minimizing common mode deviations from linear velocities. The velocities of those four local permanent stations are stable and no significant coseismic offsets were recorded on the coordinate time series (Figure 3a). Then coordinates of all 125 GPS stations in northern Taiwan were calculated from the positions of four local stations whose coordinates were derived from the *a priori* positions and velocities. The results indicate horizontal uncertainties of station coordinates are 3–4 mm and the vertical uncertainties are 10–40 mm. Because of a relatively large uncertainty of the vertical velocities in our results, we only discuss horizontal velocities in this paper.

4. GPS Velocity Field in Northern Taiwan

[10] In order to better illustrate tectonic deformation in northern Taiwan, we first intended to estimate secular velocities of GPS stations. We searched best fits of stations velocities in the coordinate time series from 1995 to 2005 with a linear function using the least squares method (Figure 3b). However, within this time period, the 31 March 2002 M_L = 6.8 Hualien earthquake

Table 1. Station Velocities Relative to Paisha, Penghu in Northern Taiwan[a]

Station	Longitude (°)	Latitude (°)	V_E (mm/yr)	V_N (mm/yr)	V_Z (mm/yr)	Err_E (mm/yr)	Err_N (mm/yr)	Err_Z (mm/yr)	V (mm/yr)	Azi (°)	N_1	N_2	Data Period (yr)
BANC	***121.442***	***24.998***	***0.53***	***3.91***	***−2.33***	***0.02***	***0.02***	***0.03***	***3.95***	***7.72***	***12***	***229***	***1995.3–2005.8***
N001	121.553	25.171	0.35	1.56	−3.30	0.50	0.72	3.81	1.60	12.65	4	8	1995.3–2004.5
N002	121.478	25.144	−0.08	1.85	−2.80	0.38	0.35	3.96	1.85	357.52	4	10	1995.3–2004.5
N003	121.636	25.023	5.47	0.56	−5.03	0.80	0.56	3.39	5.50	84.15	4	10	1995.3–2004.5
N004	121.866	25.093	0.13	0.75	−4.10	0.70	0.75	5.49	0.76	9.83	5	9	1995.3–2004.6
N011	121.292	25.103	−1.82	1.83	0.54	0.40	0.18	3.93	2.58	315.16	8	30	1995.3–2005.6
N012	121.384	24.996	1.05	4.44	0.21	0.77	0.38	3.56	4.56	13.31	6	19	1995.3–2005.6
N013	121.076	25.038	0.34	−0.68	−17.13	3.32	0.79	16.29	0.76	153.43	4	10	1995.3–2002.8
N020	121.512	25.285	−0.94	0.77	3.40	0.38	0.45	7.39	1.22	309.32	7	14	1995.3–2005.6
N021	120.974	24.874	0.06	−0.11	8.37	0.62	0.62	11.91	0.13	151.39	6	13	1995.3–2004.6
N022	121.304	24.693	−1.63	8.20	3.15	0.86	1.04	7.09	8.36	348.76	4	11	2000.3–2005.6
N023	121.050	24.680	−1.25	5.86	−1.37	0.92	0.52	2.97	5.99	347.96	6	15	1995.3–2005.1
N028	120.944	24.786	1.08	−0.92	5.53	0.55	0.52	3.76	1.42	130.43	6	18	1996.1–2004.7
N035	121.999	25.006	−0.24	−1.02	−5.86	0.85	0.41	2.97	1.05	193.24	8	17	1995.4–2005.6
N039	121.744	24.805	1.40	−0.06	−6.81	0.54	0.44	4.48	1.40	92.45	7	22	1995.5–2005.6
N040	121.564	24.509	12.45	8.32	−1.59	0.88	0.53	2.99	14.97	56.25	3	8	1995.4–2005.5
N041	121.761	24.538	23.56	−17.06	−4.87	2.24	1.64	2.93	29.09	125.91	4	8	1995.4–2005.6
N043	121.549	24.993	2.80	1.61	−3.80	1.71	0.70	7.36	3.23	60.10	3	8	1995.9–2002.8
N050	121.953	24.842	2.72	−10.02	−23.20	1.86	0.60	22.09	10.38	164.81	3	7	1995.4–2000.4
N052	121.868	24.594	22.68	−33.98	−1.83	0.99	0.71	7.89	40.85	146.28	8	18	1995.5–2005.6
N053	121.778	24.397	9.37	−16.96	−4.08	1.12	0.64	7.78	19.38	151.08	6	20	1995.4–2001.5
N054	121.492	24.781	−0.20	7.85	−11.04	0.40	0.57	24.19	7.85	358.54	6	10	1995.4–2005.6
N068	121.776	25.143	3.31	−0.48	−4.83	1.12	0.63	4.78	3.34	98.25	5	17	1995.3–2004.6
N085	121.334	24.812	−0.32	6.70	3.41	0.29	0.35	11.75	6.71	357.27	7	24	1995.3–2005.6
N090	121.619	24.659	11.49	2.40	−4.19	0.50	0.40	4.42	11.74	78.20	6	16	1995.5–2005.7
N091	121.252	25.002	−0.53	2.70	−9.91	0.47	0.64	7.30	2.75	348.89	4	11	1999.8–2005.6
N096	121.802	24.870	−0.12	−0.37	−3.52	0.46	0.41	3.71	0.39	197.97	7	16	1995.4–2005.6
N301	121.479	24.997	1.05	1.59	10.57	0.54	0.41	8.40	1.91	33.44	4	9	1996.1–2005.6
N307	121.692	24.983	−2.17	−1.29	−12.39	0.83	0.44	4.28	2.52	239.27	3	5	1996.1–2005.6
N317	121.199	24.718	−3.10	10.14	5.39	0.69	0.50	6.15	10.60	343.00	2	3	1996.1–2005.7
N321	121.543	25.148	1.92	2.17	9.02	0.55	0.49	4.97	2.90	41.50	4	7	1996.1–2005.6
N324	121.752	25.119	3.80	0.37	4.79	0.53	0.55	2.68	3.82	84.44	4	11	1996.1–2004.6
N325	121.578	25.188	2.09	1.31	0.39	0.38	0.66	3.66	2.47	57.92	4	11	1996.1–2005.6
N327	121.817	24.796	7.39	−5.91	−14.50	1.90	0.69	3.46	9.46	128.65	2	3	1996.1–2001.5
N328	121.692	24.911	0.80	1.65	2.90	0.42	0.36	3.43	1.83	25.87	4	10	1996.1–2005.6
N329	121.074	24.803	−2.61	4.09	1.65	0.29	0.56	2.88	4.85	327.46	2	5	1996.1–2004.7
N333	121.267	24.729	−2.73	11.14	7.36	0.67	0.60	3.73	11.47	346.23	3	8	1996.1–2005.6
N334	120.930	24.733	−1.93	3.42	−3.32	1.51	2.03	18.79	3.93	330.56	4	8	2001.3–2005.1
N336	120.989	24.918	−1.72	1.04	−10.67	0.56	0.53	4.45	2.01	301.16	2	7	1996.1–2005.0
N337	121.566	24.938	−0.15	4.64	4.77	0.44	0.30	2.31	4.64	358.15	4	9	1996.1–2005.6
N339	121.918	25.001	0.35	−0.49	−5.23	0.60	0.70	4.38	0.60	144.46	4	11	1996.1–2005.6
N345	121.607	25.129	2.92	1.67	0.67	0.44	0.54	4.23	3.36	60.23	3	6	1996.1–2005.6
N354	121.325	25.026	−3.36	2.34	0.67	1.39	0.53	3.49	4.09	304.85	3	8	1996.1–2004.5
N355	121.699	25.109	0.49	2.44	5.68	0.80	0.29	2.52	2.49	11.36	3	6	1996.1–2004.6
N363	121.670	25.177	2.55	0.96	1.52	1.48	0.87	6.25	2.72	69.37	4	8	1996.1–2005.6
N364	121.529	25.084	1.88	2.48	8.58	0.30	0.40	5.17	3.11	37.16	4	7	1996.1–2005.6
N365	121.781	25.071	1.63	0.57	−11.48	0.65	0.24	2.62	1.73	70.73	3	7	1996.1–2005.6
N366	121.736	24.637	23.47	−7.62	−1.05	2.87	1.03	5.03	24.68	107.99	3	10	1996.1–2005.7
N367	121.476	25.174	0.13	1.05	0.99	0.71	0.65	5.72	1.06	7.06	3	6	1996.1–2004.5
N369	121.146	24.741	−9.68	6.42	0.89	2.46	0.72	8.82	11.62	303.55	3	7	1996.1–2004.5
N370	121.036	24.972	−0.72	1.17	3.18	0.49	0.45	2.55	1.37	328.39	3	9	1996.1–2005.6
N372	121.523	24.988	−0.53	5.43	5.40	0.32	1.09	4.26	5.46	354.43	3	5	1996.1–2004.5
N379	120.985	24.793	−0.95	−0.24	1.43	0.44	0.34	4.27	0.98	255.82	3	8	1996.1–2004.8
N383	121.431	25.180	−1.42	2.38	9.61	0.44	0.55	4.13	2.77	329.18	2	7	1996.1–2004.6
N385	121.565	25.019	2.97	2.24	2.04	0.40	0.92	3.24	3.72	52.98	3	7	1996.1–2004.5
N392	121.648	24.943	0.03	2.56	2.51	0.30	0.35	1.31	2.56	0.67	4	7	1996.1–2005.6
N395	121.575	24.967	0.66	4.68	3.19	0.52	0.33	11.42	4.73	8.03	4	6	1996.1–2005.6
N396	121.087	24.840	−4.26	2.69	4.29	0.18	0.46	2.00	5.04	302.27	3	6	1996.1–2005.6
N397	121.046	24.821	−2.19	3.27	5.03	0.46	0.48	2.37	3.94	326.19	2	7	1996.1–2004.7
N398	121.226	24.741	−4.25	10.65	3.86	0.75	0.62	4.42	11.47	338.24	2	4	1996.1–2004.5
N401	121.494	25.212	−1.39	3.28	3.21	3.10	1.04	1.41	3.56	337.03	2	4	1996.1–2004.5
N405	121.537	25.265	0.36	2.24	7.35	0.41	0.17	5.52	2.27	9.13	3	5	1996.1–2005.6
N407	121.791	24.660	20.02	−14.02	−2.07	0.37	0.59	4.35	24.44	125.00	3	7	1996.1–2005.6
N421	121.074	24.942	−1.23	1.60	1.96	0.47	0.21	2.02	2.02	322.45	3	7	1996.1–2005.6
N424	121.397	24.925	−0.17	5.71	16.13	1.01	0.86	10.28	5.71	358.29	4	8	1996.1–2005.6
N429	121.500	24.617	3.86	5.12	9.02	1.92	1.70	13.63	6.41	37.01	3	8	2002.7–2005.6
N432	121.160	25.050	−1.11	1.97	−3.41	0.44	0.30	3.63	2.26	330.60	3	7	1996.1–2005.6
N437	120.999	24.719	−1.51	0.16	−2.15	0.87	0.27	3.55	1.52	276.05	3	9	1996.1–2004.8
N467	121.395	24.685	−4.07	6.18	2.44	1.30	2.24	11.38	7.40	326.63	3	7	2002.7–2005.7
N470	121.835	24.887	0.98	−1.18	−4.99	1.00	0.76	4.07	1.53	140.29	4	8	1996.1–2005.6
N480	121.172	24.889	−1.15	3.74	3.13	0.55	0.47	3.58	3.91	342.91	4	9	1996.1–2005.6
N483	121.188	24.866	−3.47	3.88	−11.07	0.43	0.50	5.16	5.21	318.19	3	5	1996.1–2004.5

Table 1. (continued)

Station	Longitude (°)	Latitude (°)	V_E (mm/yr)	V_N (mm/yr)	V_Z (mm/yr)	Err_E (mm/yr)	Err_N (mm/yr)	Err_Z (mm/yr)	V (mm/yr)	Azi (°)	N_1	N_2	Data Period (yr)
N485	121.921	25.065	0.93	−1.57	−2.42	0.72	0.66	0.91	1.82	149.36	3	6	1996.1–2004.6
N488	121.138	24.765	−1.99	6.22	12.86	0.61	0.47	6.19	6.53	342.26	3	7	1996.1–2004.7
N524	121.806	25.130	0.51	0.31	5.43	0.93	1.01	3.95	0.60	58.71	3	4	1996.1–2004.6
N525	121.486	24.574	3.44	6.71	−11.37	1.91	1.90	43.41	7.54	27.14	3	6	2002.7–2005.6
N529	121.518	25.127	1.51	1.78	12.16	0.43	0.27	4.32	2.33	40.31	3	6	1996.1–2004.5
N533	121.453	24.792	0.92	7.42	16.16	0.20	0.42	11.53	7.48	7.07	3	4	1996.1–2005.6
N540	121.144	24.817	−1.64	3.71	−0.29	0.19	0.21	6.42	4.06	336.15	2	6	1996.1–2004.7
N637	121.678	24.694	9.86	−1.43	−2.76	0.91	0.25	3.57	9.96	98.25	3	10	1996.1–2005.7
N654	121.496	24.969	0.70	3.50	4.59	0.12	0.41	0.38	3.57	11.31	3	4	1996.1–2005.6
N683	121.640	24.995	2.70	1.12	9.09	0.56	0.29	0.89	2.92	67.47	2	6	1996.1–2004.5
N701	121.620	24.967	0.92	2.26	5.31	0.37	0.29	4.16	2.44	22.15	3	9	1996.1–2004.6
N727	121.483	25.257	−0.62	1.17	12.14	1.36	0.84	16.49	1.32	332.08	2	3	1996.1–2004.5
N741	121.601	24.999	1.82	1.91	6.75	0.15	0.21	1.24	2.64	43.62	2	4	1996.1–2004.5
N773	121.510	25.106	2.42	2.80	15.90	0.61	0.41	5.57	3.70	40.84	3	6	1996.1–2004.5
N782	121.246	25.038	−6.38	2.49	−1.71	3.82	0.49	2.59	6.85	291.32	3	7	1996.1–2004.7
N801	121.723	25.121	2.68	1.43	4.28	0.78	0.71	17.76	3.04	61.92	4	9	1996.1–2004.5
N802	121.534	25.064	0.98	3.75	8.32	0.27	0.59	1.49	3.88	14.65	3	9	1996.1–2004.5
N803	121.452	25.037	2.87	3.38	2.23	0.52	0.69	8.13	4.43	40.34	4	13	1996.1–2004.6
N804	121.301	24.994	−3.36	3.06	−1.08	1.73	0.68	5.41	4.54	312.32	4	8	1996.1–2005.6
N806	120.976	24.817	−2.03	−0.57	3.93	0.25	0.49	3.58	2.11	254.32	4	11	1996.1–2004.8
N807	121.091	24.736	−2.93	6.64	1.19	1.20	0.34	3.82	7.26	336.19	3	4	1996.1–2004.5
N808	121.542	24.967	−0.21	4.47	15.71	0.68	0.35	11.98	4.47	357.31	4	9	1997.9–2004.5
N813	121.386	25.115	0.55	2.66	7.61	1.25	0.17	4.16	2.72	11.68	2	3	1996.1–2004.5
N819	121.710	25.159	4.84	1.22	7.23	1.08	0.62	6.92	4.99	75.85	4	7	1996.1–2004.5
N828	121.624	25.053	1.40	1.30	−6.35	0.51	0.36	2.78	1.91	47.12	3	12	1996.1–2004.6
N899	121.296	25.067	−3.41	2.53	−11.29	0.37	0.49	4.74	4.25	306.57	3	8	1996.1–2004.7
N901	121.695	25.210	2.54	0.31	2.05	1.16	0.63	6.29	2.56	83.04	5	9	1996.1–2005.6
N902	121.394	25.038	−1.80	4.65	−7.90	0.69	0.51	3.99	4.99	338.84	3	8	1996.1–2004.8
N903	121.327	25.116	−1.39	1.55	6.99	0.68	0.42	3.55	2.08	318.12	4	7	1996.1–2004.6
N904	121.919	25.121	0.57	−0.38	2.77	0.33	0.82	6.22	0.69	123.69	3	6	1996.1–2004.5
N905	121.026	24.880	−2.08	0.17	−9.25	0.28	0.19	2.03	2.09	274.67	3	7	1996.1–2005.6
N907	121.149	24.905	−2.31	3.93	2.46	0.75	0.52	3.45	4.56	329.55	4	10	1996.1–2005.6
N908	121.035	24.908	−4.27	2.38	−15.10	0.39	0.30	4.09	4.89	299.13	2	4	1996.1–2004.8
N910	121.180	24.796	−1.78	6.53	−17.08	0.83	0.34	6.69	6.77	344.75	3	7	1996.1–2004.6
N911	121.128	24.696	−8.00	9.83	−0.45	1.27	0.89	6.84	12.67	320.86	4	11	2002.7–2005.7
N912	121.803	24.691	10.16	−10.95	−5.54	0.68	0.35	4.68	14.94	137.14	3	5	1996.1–2005.6
N914	121.808	24.638	24.97	−15.20	1.56	0.82	0.53	4.12	29.23	121.33	3	8	1996.1–2005.6
N915	121.198	24.957	−0.77	5.18	−0.10	0.28	0.16	1.90	5.24	351.54	2	6	1996.1–2002.8
N916	121.264	24.893	−5.00	4.68	1.66	0.99	0.82	2.67	6.85	313.11	4	12	1996.1–2005.6
N917	121.223	24.861	−6.39	6.25	0.12	1.33	0.64	4.37	8.94	314.37	3	8	1996.1–2004.6
N918	121.080	24.767	−2.06	4.94	0.46	0.14	0.36	5.88	5.35	337.36	3	8	1996.1–2004.8
N919	121.037	24.711	0.96	−1.28	−4.59	1.13	0.38	2.25	1.60	143.13	3	8	1996.1–2004.6
N949	121.831	24.671	10.97	−18.65	−11.89	2.01	0.63	9.65	21.64	149.54	4	7	1996.1–2005.6
N951	121.512	24.939	−0.11	5.79	15.11	0.62	0.60	4.90	5.79	358.91	4	7	1996.1–2005.6
N958	121.326	25.092	−0.94	2.72	10.08	0.39	0.24	2.97	2.88	340.94	2	4	1996.1–2004.6
N971	121.696	24.663	16.59	−2.22	−0.13	0.33	0.18	3.28	16.74	97.62	3	6	1996.1–2005.7
N982	121.457	25.113	−0.37	2.52	5.99	2.16	0.26	2.51	2.55	351.65	4	9	1996.1–2004.5
N988	121.849	25.045	0.97	−0.80	−7.10	0.42	0.12	4.10	1.26	129.51	3	5	1996.1–2005.6
N989	121.679	25.080	0.50	−0.71	1.47	1.13	0.86	2.15	0.87	144.85	4	7	1996.1–2005.6
TAIW	***121.537***	***25.021***	***2.54***	***1.98***	***−6.11***	***0.56***	***0.74***	***2.73***	***3.22***	***52.06***	***4***	***44***	***1995.3–1997.9***
TNML	***120.987***	***24.798***	***−2.58***	***3.50***	***−4.66***	***0.09***	***0.08***	***0.45***	***4.35***	***323.60***	***6***	***191***	***2001.5–2005.8***
TWTF	***121.165***	***24.954***	***−1.34***	***1.22***	***−8.18***	***0.11***	***0.10***	***0.80***	***1.81***	***312.32***	***5***	***173***	***2002.7–2005.8***
YMSM	***121.574***	***25.166***	***1.60***	***1.96***	***−4.47***	***0.05***	***0.06***	***0.30***	***2.53***	***39.23***	***13***	***227***	***1995.3–2005.8***

[a] V_N, V_E, and V_Z are north, east, and vertical component of interseismic velocities, respectively; Err_N, Err_E, and Err_Z are errors in north, east, and vertical component, respectively; V is the station horizontal velocity; Azi is the azimuth of V; N_1 is the number of sessions; and N_2 is the number of campaigns. Permanent stations are shown in bold and italic.

(Figure 1), an offshore earthquake in eastern Taiwan, produced significant coseismic offsets up to 55 mm in northern Taiwan [*Chen et al.*, 2002]. As a consequence, we adopted an inversion technique by using the kinematic model software Poly3D [*Thomas*, 1993] to estimate the coseismic offset corrections for the 2002 earthquake. The fault geometry is constrained by the focal mechanism solution and the aftershocks distribution from the Broadband Array in Taiwan for Seismology (BATS). Due to absence of precise information to identify the fault length and fault width, the optimal fault length and width were searched by genetic algorithms (GA). GA is an optimization method in terms of an analogy originally for biological evolution, reproduction, crossovers and mutations, in order to search the optimal solutions in multiparametric spaces [*Goldberg*, 1989]. The GA works on a set of models at the same time. We used a FORTRAN version of a genetic algorithm GAFORTRAN version 1.7 developed by David L. Carroll. Crossover is uniform with the probability equal to 0.5. The uniform crossover means the same probability of

crossover is given to each parameter of the model. Mutations occurred with the probability 0.04. By neglecting postseismic effect, that is, assuming the secular motions before and after the earthquake are consistent, the secular velocity (Vs) is expressed as

$$V_s = (V \times \Delta T - D)/\Delta T, \quad (1)$$

where V denotes the uncorrected velocity, ΔT is the observation span, and D is correction of coseismic offset.

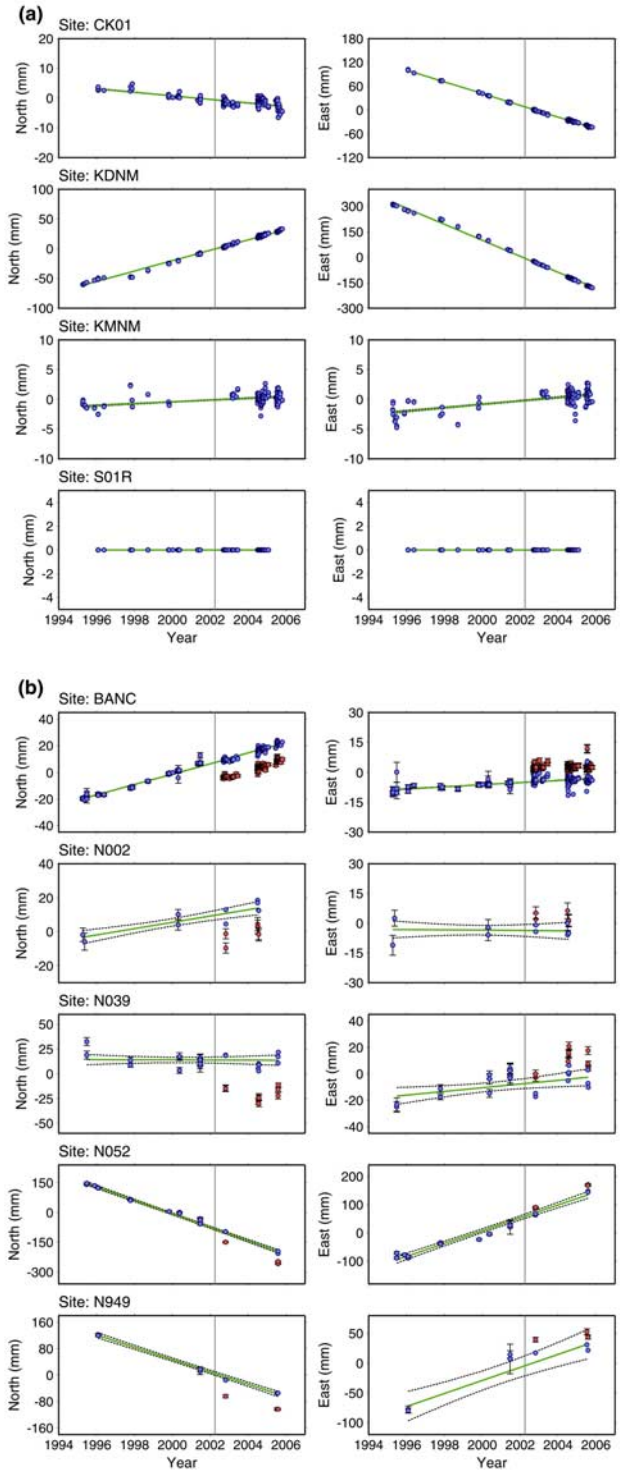

For the standard deviation of a velocity field, in addition to the uncertainties associated with the least squares estimation of velocities (σ_{ls}), we also considered the effect from daily coordinate variation (σ_{cv}) presented in the coordinate time series. The effect of daily coordinate variation σ_{cv} is $mis/2$, where mis is the residual of calculations and observations for the coordinate time series on east, north, and vertical component, respectively. Then the uncertainty σ of a velocity for each component is re-estimated by $\sigma = (\sigma_{ls}^2 \times \sigma_{cv}^2)^{1/2}$ (Figure 3). Table 1 lists all 125 GPS stations used for GPS velocity estimates in the study.

[11] We reconstructed the map of the GPS velocity field for all 125 stations in northern Taiwan (Figure 2) with respect to the Chinese continental margin station, S01R, at Penghu Island in the Taiwan Strait (Figure 1). The GPS velocities were estimated using daily coordinates from April 1995 to October 2005. Vectors of the GPS velocity field from west to east form an asymmetric fan shape and gradually change clockwise from NW to SE in direction (Figure 2). From east to west, magnitudes of the horizontal velocities from the Central Range to the Taiwan Strait shoreline generally decrease from ~11.5 mm/yr to ~0.0 mm/yr (Figure 2).

[12] In terms of spatial variation of the velocity field and locations of active structures, from west to east, northern Taiwan is divided into four domains. First, the stations west of the surface projection of the western boundary of the subducting Philippine Sea plate (i.e., the waning collision area) generally move in a NW direction, duplicating the NW converging Luzon arc of the Philippine Sea plate. The velocities decrease westward from 11.5 mm/yr to 0.2 mm/yr. Second, in the transition zone, the GPS vectors show an apparent clockwise rotation. In more detail, from the north in the small area between the Nankan fault (NKNF) and Chinshan–Shanchiao faults, GPS vectors from west to east show a slight clockwise rotation of 30° (from 303° to 332°) with magnitudes of 1.3–4.3 mm/yr. Further south between the Chinshan–Shanchiao fault and the Ilan plain or the eastern outer range of the transition zone, GPS velocities from west to east rotate clockwise of more than 90° (from N to SE directions). Velocity magnitudes range from 5.5 m/yr to 1.2 mm/yr in this area. Finally, in the inner range of the transition zone, velocities from north to south increase from 1.1 mm/yr to 41.6 mm/yr and the azimuths from

Figure 3. Coordinate time series of the selected GPS stations. Red circles are original observations. Blue circles indicate the corrected data in which the coseismic offsets of 2002 Hualien, Taiwan offshore earthquake were removed. The gray lines represent the occurrence epoch of the 2002 Hualien, Taiwan offshore earthquake. Green lines are the best-fitting lines using the least squares method. Black dashed lines denote a 95% confidence interval. (a) Coordinate time series of the constrained local permanent GPS stations. (b) Coordinate time series of the selected campaign-surveyed GPS stations. The coordinate time series of the station BANC denotes the best case while the time series of the site N949 shows the worst case.

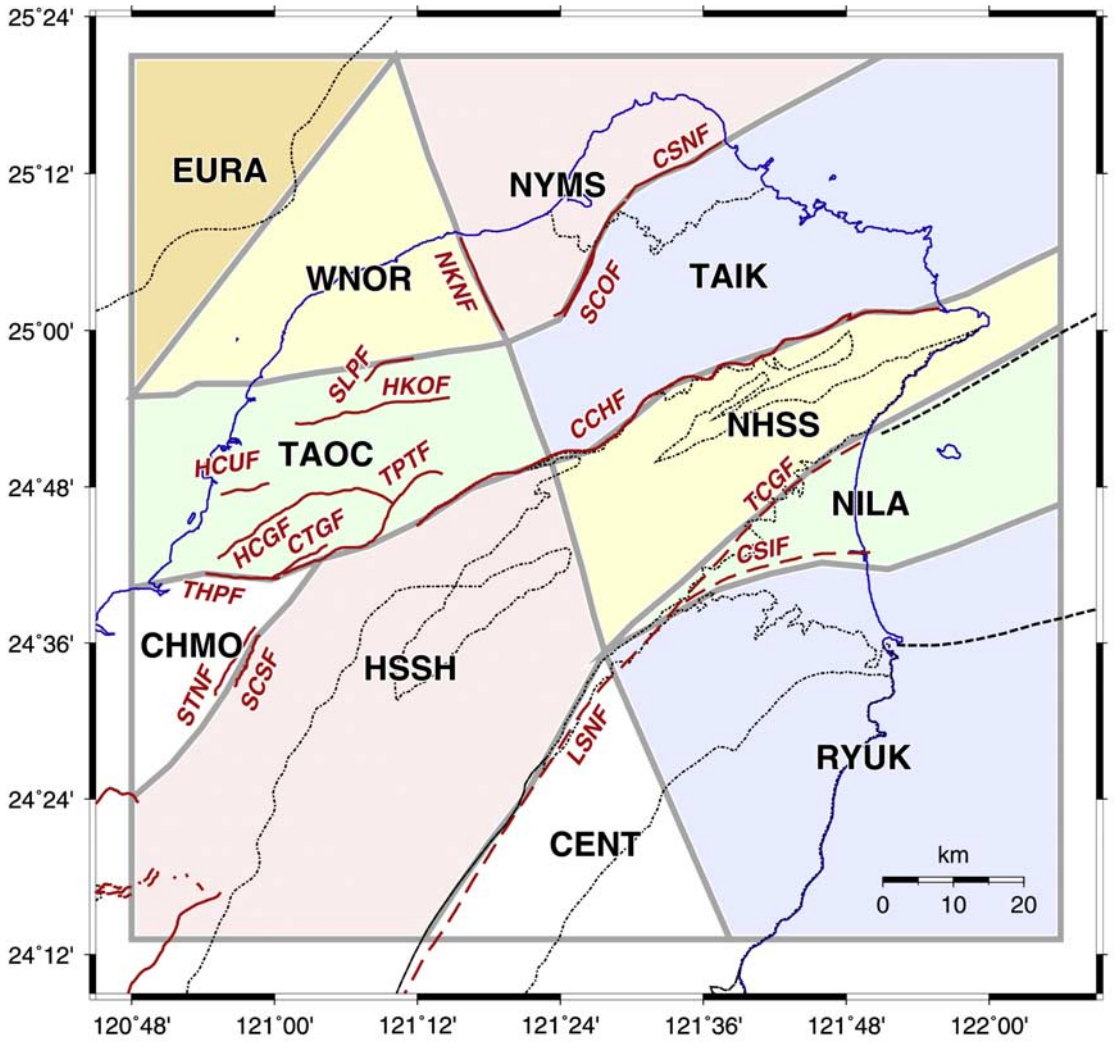

Figure 4. Tectonic block configuration of northern Taiwan used in this paper. Thick gray lines show the block boundaries. Block names are represented in black bold. Red lines are the positions of major faults.

west to east gradually change clockwise of more than 120° (from 027° to 151°).

5. Elastic Block Modeling for Northern Taiwan

[13] Interseismic deformation at the plate boundary zone is primarily dominated by the motions of tectonic blocks and interseismic coupling on faults [e.g., *Savage*, 1983]. In order to interpret the GPS velocity field in northern Taiwan, we implemented a method developed by *McCaffrey* [2002] that matches the GPS velocity field with rotations of rigid blocks and the elastic strain rates resulting from friction on block-bounding faults. In addition to the strain rates induced by block-bounding faults, the nonrecoverable strain rates (i.e., the permanent strain rates) are assumed to represent the coupling of faults inside the tectonic blocks [*McCaffrey*, 2005]. Then the nonlinear inversion applies simulated annealing to a downhill simplex minimization [*Press et al.*, 1989] to invert the GPS velocity field for simultaneously estimating the Euler pole locations and angular velocities of tectonic blocks, coupling coefficients on block-bounding faults and permanent strain rates within the blocks. Because of friction on the fault plane, the short-term (interseismic) slip rates across most faults are less than the long-term (over many earthquake cycles) slip rates expected from the relative motion of the adjacent tectonic blocks. To describe the influence of faults on the velocity field, a pure scalar quantity is represented with ϕ (coupling coefficient) [*McCaffrey*, 2002]. If $\boldsymbol{V}$ is the long-term slip rate vector on the fault and $\boldsymbol{V}_c$ is the short-term creeping rate vector, then $\phi = 1 - \boldsymbol{V}_c/\boldsymbol{V}$. When $\phi = 0$, creep occurs at the long-term fault slip rate and when $\phi = 1$, the fault is totally stuck in the interseismic period. In this inversion, we estimated ϕ at grids of predefined nodes on the block-bounding faults. The coupling coefficient ϕ is assumed as time-invariant over the 10-year span of our GPS data although ϕ may vary as a function of time. We also imposed the constraint that ϕ decreases downdip from a value of one (totally stuck) at the surface to zero (totally creeping) at the bottom of fault, because terrestrial faults in northern Taiwan reveal no evidence for aseismic surface creeping. The slip rate deficit on the fault is the scalar coupling value ϕ multiplied by the long-term slip rate $\boldsymbol{V}$. The contribution to the velocity field from slip rate deficit is calculated by a back slip model

Table 2. Euler Vectors for the Tectonic Blocks Adopted in This Study Relative to the Eurasian Plate[a]

Block	Longitude	Latitude	Rate, °/Myr	e_{max}	e_{min}	Azimuth	χ^2/N
WNOR	130.167	30.752	−0.20 ± 0.55	36.79	1.04	236	4.94
NYMS	130.167	30.752	−1.25 ± 1.61	2.91	0.20	236	2.37
TAIK	122.821	26.058	−5.05 ± 1.60	0.22	0.16	265	5.70
TAOC	121.891	24.940	−0.20 ± 0.55	36.79	1.04	236	29.60
HSSH	130.167	30.752	−2.81 ± 2.21	3.17	0.20	248	6.54
NHSS	123.997	25.884	−5.06 ± 1.60	0.22	0.16	265	5.36
NILA	121.891	24.940	−13.43 ± 40.18	1.09	0.21	131	3.89
RYUK	121.593	24.886	−47.30 ± 7.76	0.04	0.03	251	15.60

[a] e_{max}, e_{min}, and azimuth refer to the maximum and minimum standard errors of the uncertainty ellipse (in degrees), and the azimuth of the major axis, respectively. Negative rotation rates indicate clockwise motion. See Figure 4 captions for key to block name abbreviations. χ^2/N is chi-square per observations.

[*Savage*, 1983], using the formulations of *Okada* [1985] for surface displacements due to dislocations in elastic half-space. The best fit parameters are determined by minimizing data misfit, defined by reduced chi-square statistic (χ^2).

5.1. Tectonic Block and Fault Configurations Used for the Northern Taiwan

[14] In northern Taiwan 11 tectonic blocks are divided (Figure 4) based on GPS vectors, surface geology, active faults, and geometric architecture of the Philippine Sea plate. Blocks are closed, spherical polygons on the Earth's surface and cover the entire model domain (Figure 4). Each point within a block is assumed to rotate with the same angular velocity, i.e., rigid block kinematics. The boundary of the reference stable block (EURA) is defined approximately along the margin of the Kuanyin basement high, inherited from its Paleogene to Miocene extensional history on the continental margin of Eurasian plate [*Lu et*

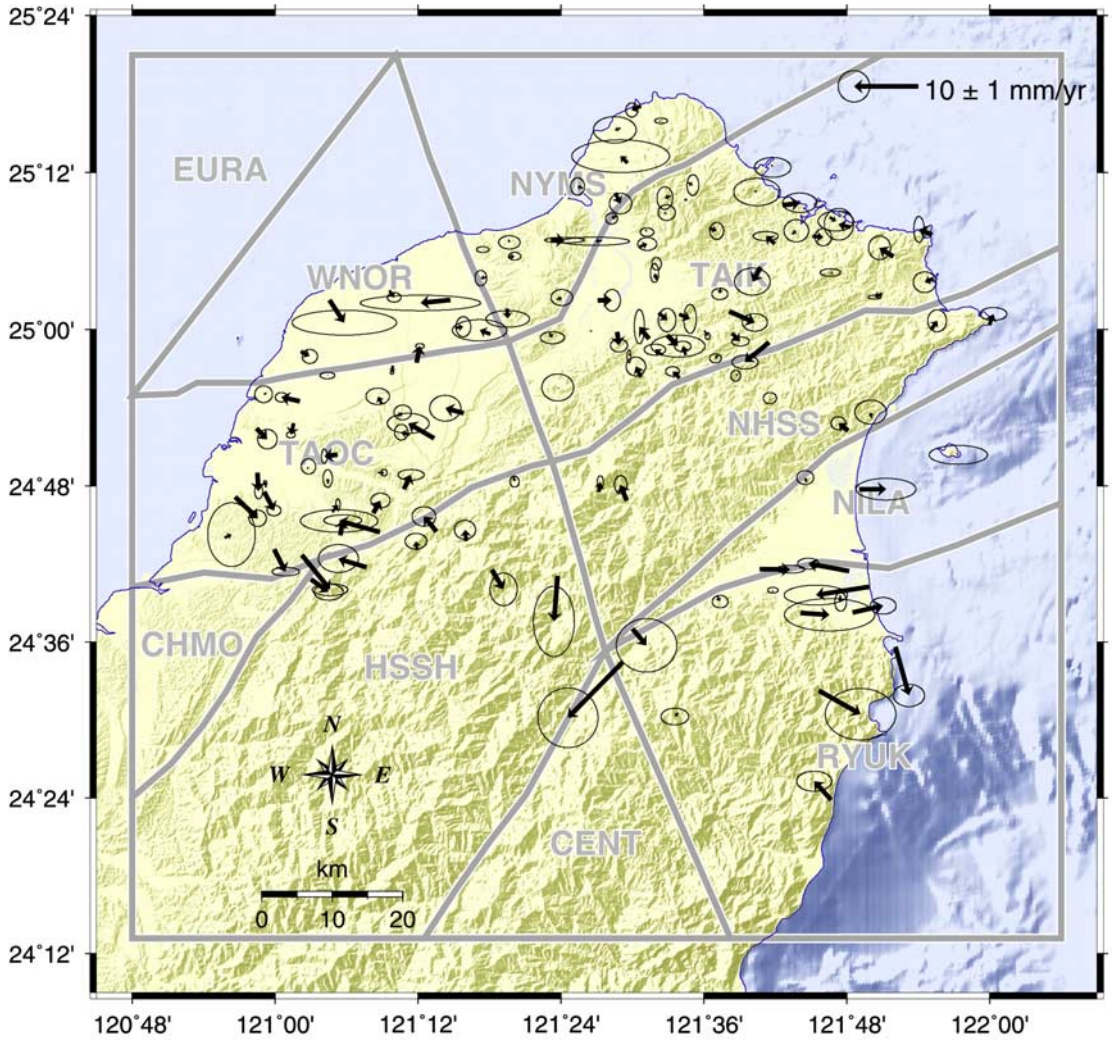

Figure 5. GPS velocity residuals for best-fitting block model with 95% confidence data uncertainties (i.e., no contribution to the uncertainties). Thick gray lines show the block boundaries.

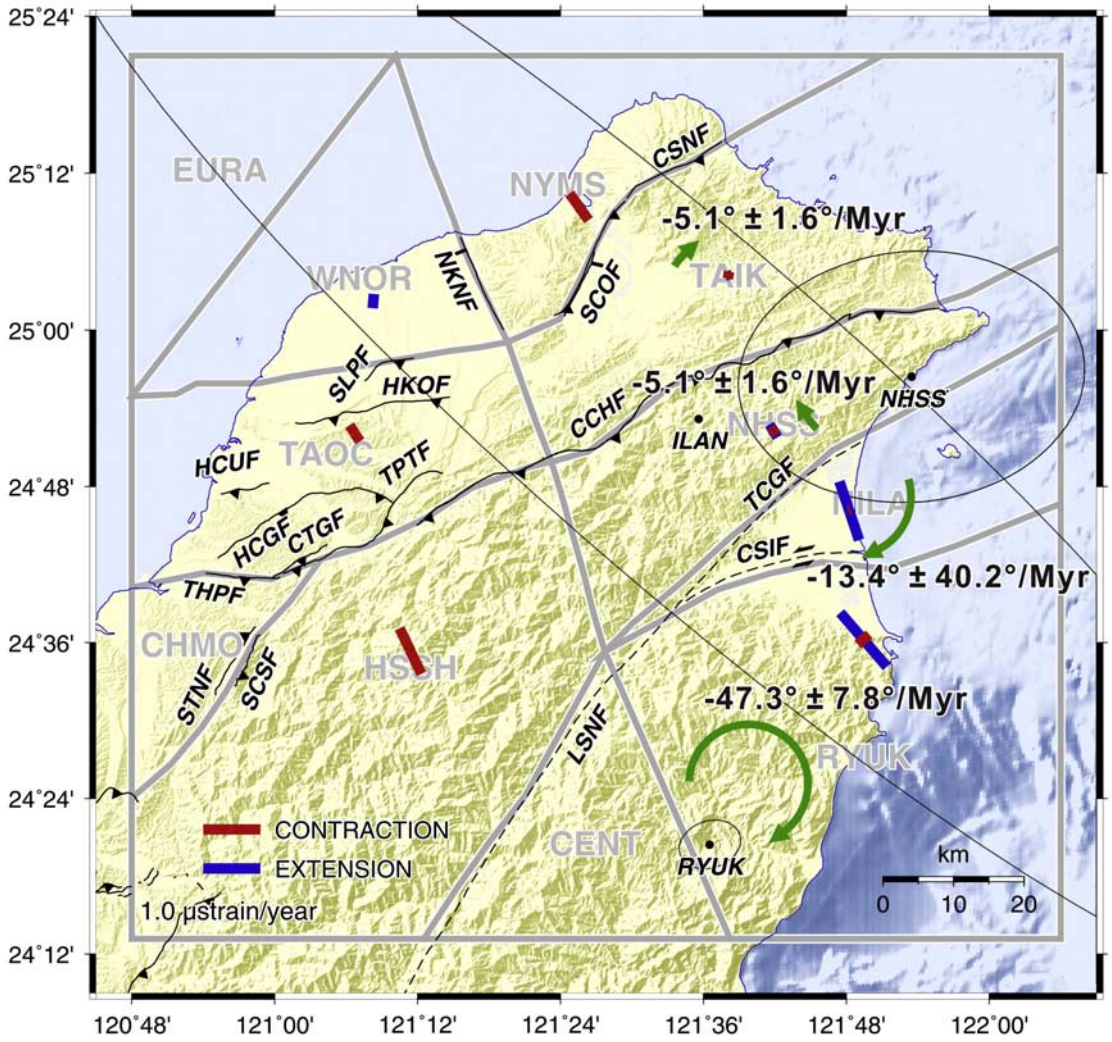

Figure 6. Locations of the Euler poles, angular velocities, and the distribution of permanent strain rates for our optimal block model. Solid dots show the locations of the Euler poles and their 95% confidence error ellipse are shown with black ellipses. The thick blue bars reflect the amount and direction of principal extension rates. The red bars reflect the principal contraction rates. The green arrows denote the rotation rates of the tectonic blocks. The rotation rates of the WNOR, NYMS, TAOC, and HSSH blocks are too small and not indicated. Thick grey lines show the block boundaries. Black lines indicate major faults.

al., 1998; *Lin et al.*, 2003]. According to the seismicity, the western boundary of the NW-subducting Philippine Sea plate, separating northern Taiwan into two groups, extends northward all the way and probably connects with the Nankan fault (NKNF). For blocks in the western group (the waning collision area), the ''NW block'' (WNOR) and the ''Taoyuan-Hsinchu block'' (TAOC) is separated by the frontal thrust (SLPF). The southern boundary of the TAOC is defined by major faults (CCHF, TPTF, and THPF) in the foothills. To the south, the Shihtan–Shenchoshen fault system (SHSF), which is the surface rupture of the 1935 M = 7.1 Taichung–Hsinchu earthquake, was adopted as the boundary between the ''Chingshui–Miaoli block'' (CHMO) and the ''Hsuehshan Range block'' (HSSH). The eastern bound of the HSSH is the Lishan fault, which separates the ''Central Range block'' (CENT) to the east. For the transition zone in the eastern group (including the outer and inner ranges of transition zone), the Chinshan–Shanchiao fault system separates the ''North Yangmingshan block'' (NYMS) to the north and the ''Taipei–Keelung block'' (TAIK) to the south. The boundary fault between the TAIK and the ''North Hsuehshan Range block'' (NHSS) is the Chuchih fault (CCHF). The southern block-bounding fault of the NHSS is the Toucheng fault (TCGF). Finally, the southeastern part of the transition zone is divided into two tectonic blocks, the ''North Ilan block'' (NILA) to the north and the ''Ryukyu block'' (RYUK) to the south, bounded by the Choshui fault (CSIF).

[15] For the eastern group, the contribution to velocities from slip rate deficit on three major faults between the blocks, including the Chinshan–Shanchaio fault, the Toucheng fault, and the Choshui fault, were estimated. The Chinshan–

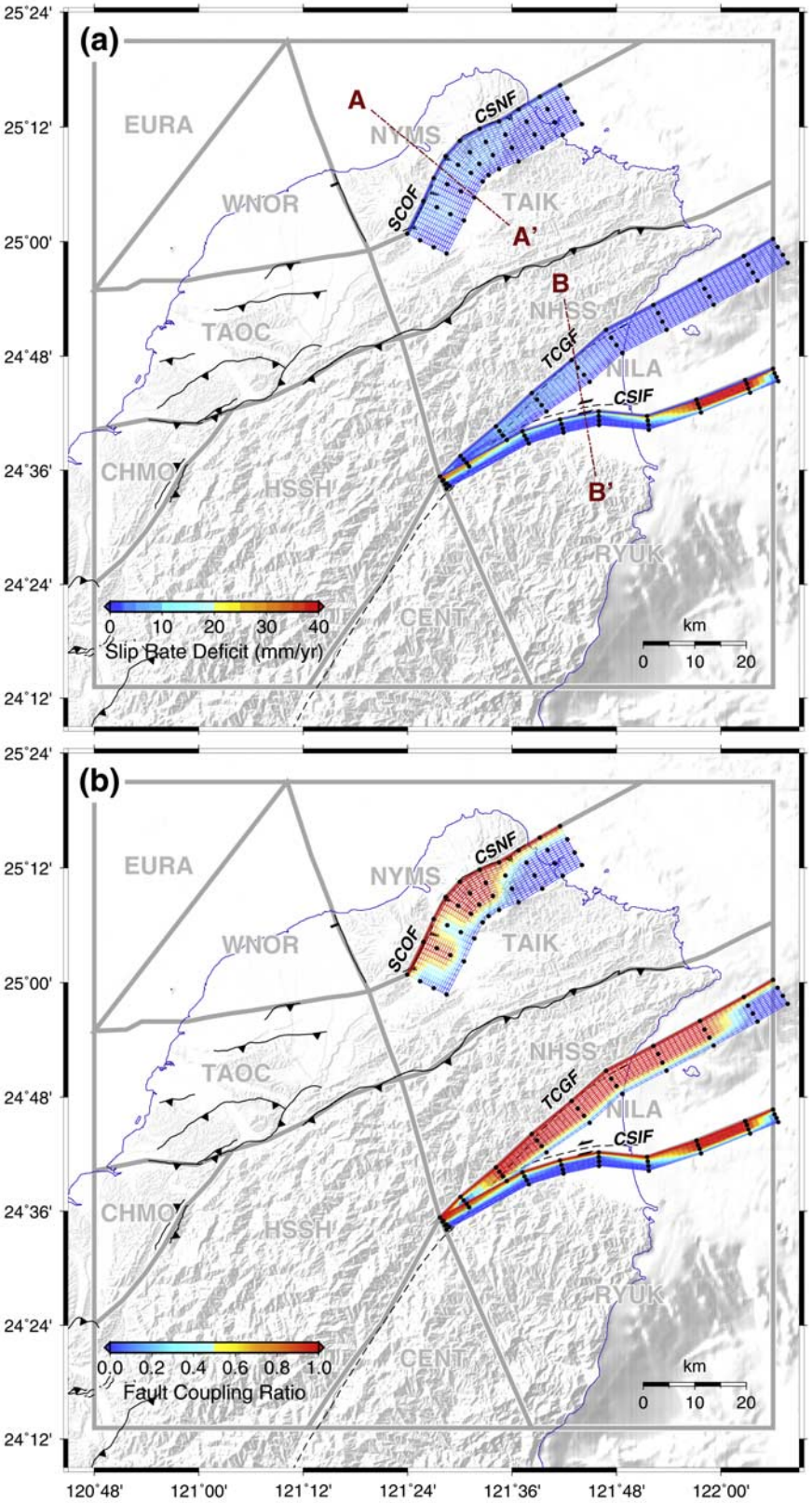
(a)
(b)
EURA
NYMS
WNOR
TAIK
TAOC
NHSS
NILA
CHMO
HSSH
RYUK
CENT
CSNF
SCOF
TCGF
CSIF
A
A'
B
B'
0 10 20 30 40
Slip Rate Deficit (mm/yr)
0.0 0.2 0.4 0.6 0.8 1.0
Fault Coupling Ratio
km
0 10 20
25°24'
25°12'
25°00'
24°48'
24°36'
24°24'
24°12'
120°48'
121°00'
121°12'
121°24'
121°36'
121°48'
122°00'

Figure 7

Table 3. Block Principal Strain Rate Estimates and 1σ Uncertainties (10^{-6}/yr)[a]

Block	ε_1	ε_2	Azimuth ε_1
WNOR	0.0012 ± 0.0301	0.123.4 ± 0.0498	−85 ± 14
NYMS	−0.2904 ± 0.0351	0.057.6 ± 0.0386	−36 ± 4
TAIK	−0.0640 ± 0.0223	0.028.3 ± 0.0246	12 ± 11
TAOC	−0.1681 ± 0.0109	0.028.9 ± 0.0130	−33 ± 2
HSSH	−0.4445 ± 0.0777	0.087.4 ± 0.0581	−26 ± 5
NHSS	−0.0791 ± 0.0417	0.129.6 ± 0.0500	−121 ± 8
NILA	−0.0221 ± 0.4281	0.541.1 ± 0.4779	−109 ± 21
RYUK	−0.1343 ± 0.0920	0.621.4 ± 0.0919	−131 ± 4

[a]Negative numbers signify contraction. Azimuth of ε_1 is in degrees east of north. See Figure 4 captions for key to block name abbreviations.

Shanchaio fault system is set at a dip of 60° to the SE based on the offshore seismic reflection profiles [*Hsiao et al.*, 1999] and earthquake scenario [*Shyu et al.*, 2005]. The Toucheng fault, as a fault system containing a zone of normal faults several km wide, is set at a dip of 70–80° to the south [*Lee*, 1991] on the basis of the geological and geomorphic evidences. The ~80° dip to the south of the Choshui fault is determined by the focal mechanisms of the 2005 earthquake doublet. In addition, we assumed the bottom for each of the three faults to be 15-km deep [*Shyu et al.*, 2005]. In other words, faults creep below 15 km.

5.2. Inversion Results

[16] We used 125 horizontal GPS velocities (250 observations) to estimate 98 parameters, including three rotation components for each of 6 rotation poles, three components of strain rate tensor for 8 tectonic blocks, and ϕ at 56 fault nodes on the block boundaries and fault configurations described in section 5.1.

[17] In our optimized model, $\chi^2 = 19.05$. Although it is relatively large, the chi-squares per observations (χ^2/N) of most blocks are less than 5.70 (Table 2). However, we can observe that a few values of χ^2/N are larger than 15.60 (Table 2), in particular on the TAOC and RYUK blocks. We interpret the large χ^2/N are mainly due to local active faults within the block, for instance, the HCGF and CTGF on the TAOC block (Figure 5). For the large χ^2/N value on the RYUK block, we tend to interpret the anomalies in the eastern RYUK block (Figure 5) as a result of the interactions among different modes of deformation act at the collision corner, e.g., extrusion, and back-arc spreading.

[18] The results of a best-fitting model are shown in Figures 6 and 7. According to the characteristics of velocity pattern and results of several tests, the WNOR and TAOC blocks in the waning collision area appeared to rotate with a similar angular velocity and Euler pole; The TAIK and NHSS blocks in the outer range of transition zone seemingly rotate with the same angular velocity and Euler pole. In addition, we didn't estimate angular velocities and strain rate tensors for the CHMO and CENT blocks because no GPS station was within observation range of these two blocks.

[19] For the blocks of the transition zone, including TAIK, NHSS, NILA, and RYUK, the rotation poles are all located within the blocks (Table 2; Figure 6). The blocks of the western group (the waning collision area) rotate along distant poles which are several hundred km northeast of the mapped area (Table 2). Rotation rates of the tectonic blocks in the waning collision area are minor (<3.0°/Myr), especially for the WNOR and TAOC blocks, which show negligible block rotation (−0.2°/Myr). For the blocks in the transition zone, save for the rotation rate for the NYMS block which is insignificant (1.3°/Myr, clockwise), the others represent rapid to ultrarapid clockwise block rotation (TAIK and NHSS: 5.1°/Myr; NILA: 13.4°/Myr; RYUK: 47.3°/Myr).

[20] In order to assess the distributed permanent strain rate (due to coupling on faults inside the blocks), we inverted for components of the horizontal strain rate tensor for eight blocks (excluding the EURA, CHMO, and CENT blocks; Table 3). For blocks in the waning collision area, we observed that (1) an N–S extension rate of 0.12 ± 0.05 μstrain/yr in N5°E is observed in the WNOR block; (2) a NW–SE contraction rate of 0.17 ± 0.01 μstrain/yr in N147°E is found in the TAOC block.; and (3) for the HSSH block, we estimated a significant shortening rate of 0.44 ± 0.08 μstrain/yr and oriented at N154°E. For the blocks in the transition zone, we found that (1) a NW–SE contraction rate of 0.29 ± 0.04 μstrain/yr in N144°E is seen in the NYMS block; (2) the TAIK block, an insignificant shortening rate of 0.06 ± 0.02 μstrain/yr in N12°E is represented; (3) a strain rate with both shortening (0.08 ± 0.04 μstrain/yr in N59°E) and lengthening (0.13 ± 0.05 μstrain/yr in N149°E) occurs in NHSS; (4) a predominant lengthening at a rate of 0.54 ± 0.48 μstrain/yr in N162°E occurred in the NILA block; and (5) a strain rate with both a large N139°E extension at a rate of 0.62 ± 0.09 μstrain/yr and N49°E contraction at a rate of 0.13 ± 0.09 μstrain/yr occurs in the RYUK block.

[21] Generally speaking, the fault slip rate deficits are not apparent with most faults in northern Taiwan (Figure 7a). For the Chinshan–Shanchaio fault (CSNF-SCOF), we obtained ϕ values of ~1.0 at the segment near the western part and 0.0–0.5 at the eastern portion of the fault (Figure 7b). However, the slip rate deficit at the locking segment is negligible (~4.7 mm/yr; Figure 7a). For the Toucheng fault (TCGF), ϕ values of ~1.0 are estimated at all nodes on the fault plane, except for the westernmost and easternmost segments of this fault (Figure 7b). The average slip rate deficit of ~6.9 mm/yr on the fault plane is also insignificant (Figure 7a). Finally, we obtained ϕ values of ~0.0 in the inland segment of the Choshui fault (CSIF) and ~0.0 for the offshore fault segment (Figure 7b). The average slip rate

Figure 7. (a) Magnitudes of slip rate deficits on the Chinshan–Sanchiao fault, the Toucheng fault, and the Choshui fault in the northern Taiwan. Red dashed lines show locations of profiles in Figure 8. (b) The coupling coefficient ϕ (from 0 to 1) on the Chinshan–Sanchiao fault, the Toucheng fault, and the Choshui fault. Locations of the nodes used to specify three-dimensional fault geometries are shown as black dots that are projected vertically to the Earth's surface. The width of the faults therefore reflects the dip of the fault (steeply dipping faults appear narrow; while shallowly dipping faults appear wide). Thick gray lines show the block boundaries. Black lines are the positions of major faults.

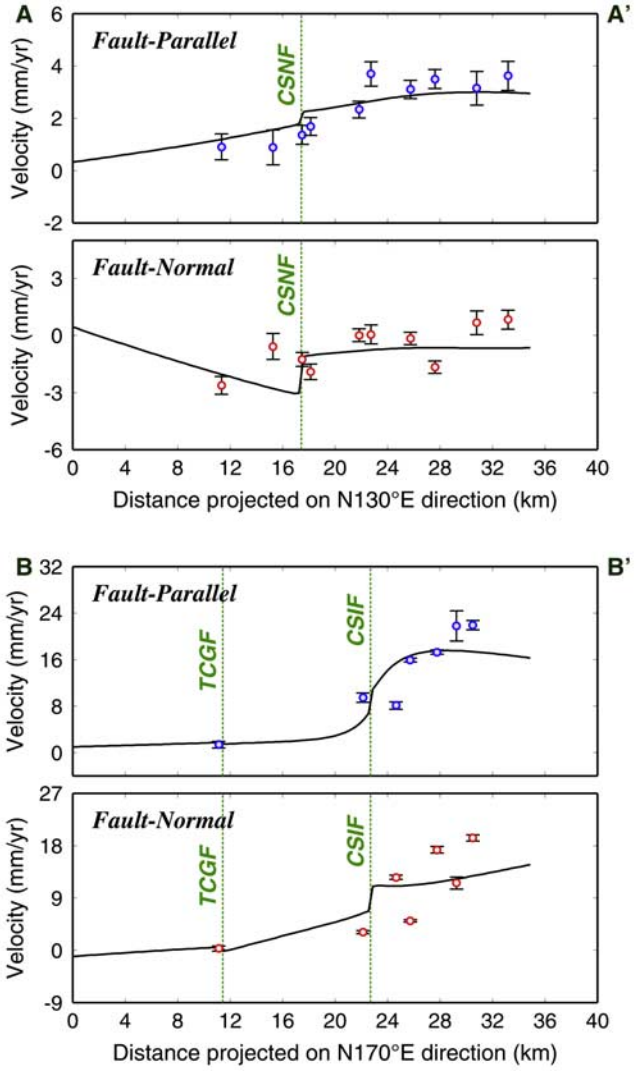

Figure 8. Velocity profiles across three major block-bounding faults. The upper panel presents the fault-parallel horizontal velocity components of selected stations, while the lower one shows the fault-normal velocity components. The green dashed lines are the locations of major block-bounding faults. Circles are GPS observations and black curves are calculations from an optimized block model. (a) The velocity profile across the Chinshan–Shanchiao fault system. (b) The velocity profile across the Toucheng fault.

deficit (~33.52 mm/yr) is significant at the locking segment of the Choshui fault (Figure 7a).

6. Discussion

6.1. Characteristics of Major Active Faults in Northern Taiwan

[22] To investigate activities of the three major active faults in northern Taiwan, including the Chinshan–Shanchiao fault system, the Toucheng fault, and the Choshui fault, we decomposed the horizontal velocity field into fault-parallel and fault-normal components to better characterize the movement behaviors of the active faults (Figure 8).

[23] Across the Chinshan–Shanchiao fault system, fault-parallel velocities from NW to SE gradually increase from nearly 0.0 mm/yr to 4.0 mm/yr (the positive sign indicates northeastward motion; Figure 8a), indicating a possible left-lateral motion of 4 mm/yr along the fault. On the other hand, for the fault-normal velocity components, velocities diminish from ~2.0 mm/yr to ~0.0 mm/yr (positive sign shows northwestward motion). Thus an extension rate of about 2.0 mm/yr is uncovered across the Chinshan–Shanchiao fault. In sum, the Chinshan–Shanchiao fault is characterized by a left-lateral strike–slip movement with significant normal motion. The ratio of dip to strike–slip motion of this fault is 0.5. The Chinshan–Shanchiao fault, which is located in metropolitan Taipei city, has received much attention and been speculated as an active normal fault due to a significant late Quaternary strata vertical offset of 800–900 m across the fault [*Teng et al.*, 2001]. Furthermore, a recent field investigation indicates an outcrop with both normal fault and strike–slip fault shear zones [*Chan et al.*, 2006]. Although no significant seismic activity has occurred along the Chinshan–Shanchiao fault during the last decades, the evidence for active faulting can be seen by the long-term geological data as well as the short-term GPS surface deformation. In addition, the moment rate deficit and the fault area derived from the block modeling are 6.99×10^{16} N m and 700 km^2, respectively. The possible moment magnitude of a future earthquake associated with the Chinshan–Shanchiao fault is ~6.85 on the basis of the empirical relationship between the moment magnitude and fault area [*Wells and Coppersmith*, 1994]. The possible recurrence interval of the Chinshan–Shanchiao fault is also estimated to be about 335 years.

[24] Between the inner and outer ranges of the transition zones, two major active faults are apparent: the Toucheng fault (TCGF) to the north and the Choshui fault (CSIF) to the south. The GPS velocity field reveals that the horizontal velocities are ~0.0 mm/yr north of the TCGF. Conversely, velocities gradually increase from 4.9 mm/yr to 19.0 mm/yr toward the south across the TCGF and the CSIF (Figure 8b). The spatial variation of the velocity field implies that the CSIF reveals a significant normal fault motion. However, the TCGF also might have a minor normal fault movement. The structure-perpendicular velocity components along NNW–SSE profile rapidly increase toward SSE direction from 4.6 mm/yr to 40.4 mm/yr (Figure 8b), indicating a left-lateral slip of about 35 mm/yr across the CSIF but no significant strike–slip movement on the TCGF. In sum, there is significant oblique normal fault motion with a left-lateral strike–slip component along the CSIF, a northeastern extension of the Lishan fault. For the TCGF, moment rate deficit and fault area inferred from the block modeling are 1.22×10^{17} N m and 1251 km^2, respectively. A possible moment magnitude for a future earthquake associated with this fault is ~7.11 based on the empirical relationship [*Wells and Coppersmith*, 1994]. Therefore the possible recurrence interval of TCGF is about 472 years. On the other hand, regarding the CSIF, an earthquake sequence of M_w = 5.5 in 2005 occurred along this E–W trending steeply S-dipping fault (Figure 1). Although no surface breaks were observed along the possible trace of the CSIF, focal mechanisms indicate a predominant left-lateral movement occurred along the fault during the earthquake. Note that the CSIF was neither well known nor considered previously as an active fault, probably because it is "blind" and covered by a

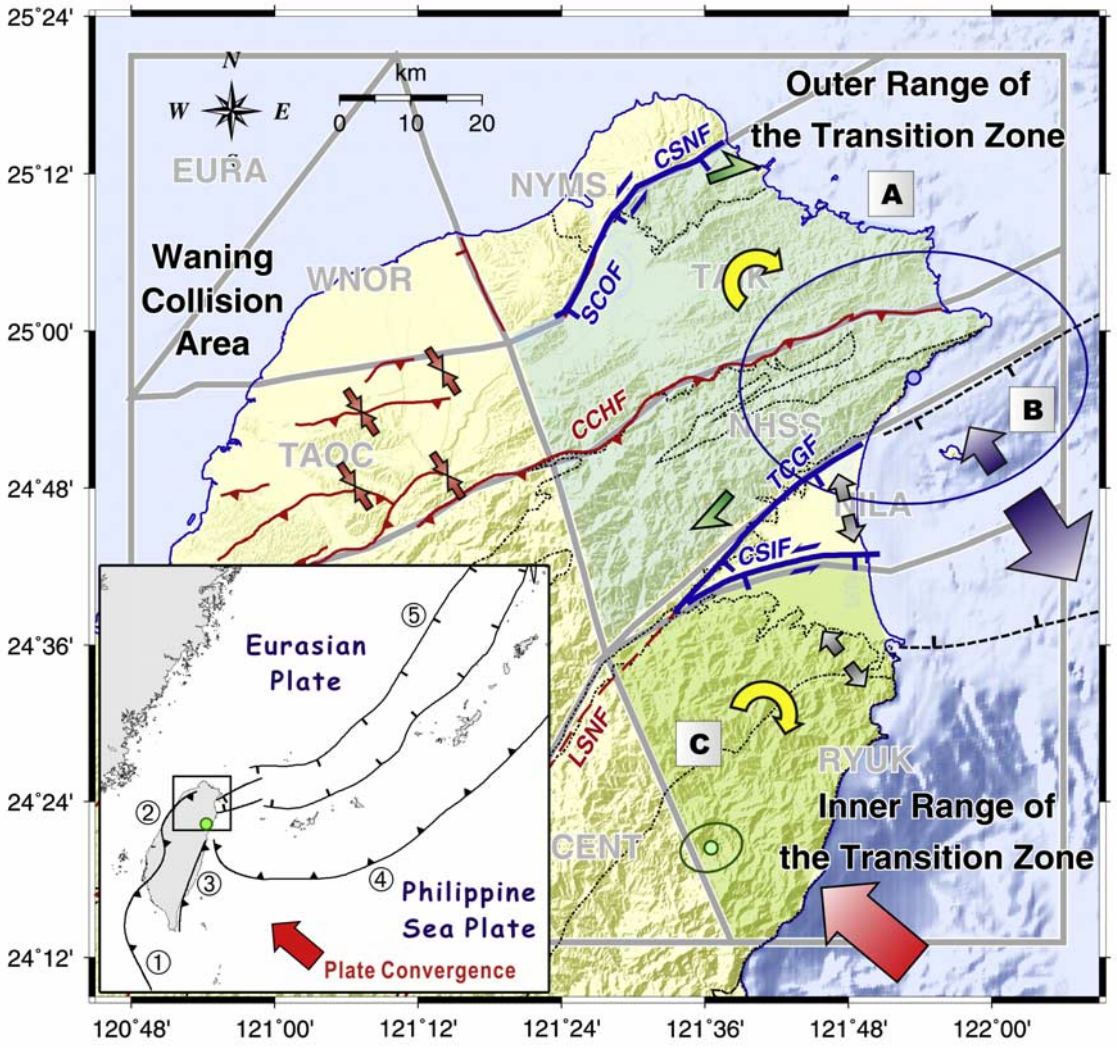

Figure 9. The tectonic model for northern Taiwan. (a) The right lateral shear zone between the Chinshan–Shanchiao fault system and the Ilan Plain (Region V). (b) The back-arc extension in the Okinawa trough. (c) The plate corner rotation as a result of collision-induced block rotation and trench retreat in the southeast of the GPS array. The thick gray lines show the block boundaries. The small red arrows represent the direction of contraction. The gray arrows denote the direction of extension. Because the southward extension rate (purple arrows in region B) is larger than northward extension and the southern purple arrow is larger than northern extension. The red arrow represents the convergence direction of the Philippine Sea plate. Blue and green circles are the Euler pole locations of the TAIK and NHSS blocks and the RYUK block, respectively. The inset shows the geotectonic framework and major structural units of the Taiwan region. The brown belt shows the position of the Okinawa trough. Numerals 1–5 denote the Manila trench, the deformation front, the Longitudinal Valley fault, the Ryukyu trench, and the Okinawa trough, respectively.

layer of alluvial deposits up to 2 km thick. The moment rate deficit and fault area of the CSIF derived from the block modeling are 6.68×10^{17} N m and 1048 km^2, respectively. Possible moment magnitude of a future earthquake associated with the CSIF is ~7.03 in terms of the empirical relationship [*Wells and Coppersmith*, 1994]. The possible recurrence interval of CSIF is about 65 years.

6.2. Block Rotations in Northern Taiwan

[25] Block modeling results show that the tectonic strain regime changes substantially from the waning collision area with NW–SE shortening and negligible block rotation to the transition zone with NW–SE lengthening and significant rotation (Figure 6). This deformation pattern is in general agreement with the geological structures under discussion [*Hu et al.*, 1996; *Teng and Lee*, 1996]. Thus the deformation of northern Taiwan deduced from decadal GPS observations is consistent with the long-term deformation. Three significant block rotations are shown in terms of block modeling (Figure 6). Because of the few GPS stations distributed within the NILA block, we focused on the meaning of block rotation for the TAIK/NHSS, and RYUK blocks.

[26] First, the TAIK/NHSS block corresponds geologically to the outer range, including the foothills and the Hsuehshan Range, of the Taiwan mountain belt. The location of the best

fitting Euler pole is near the southeastern end of the block (24.940°N, 121.891°E) with an angular velocity of 5.1° ± 1.6°/Myr (Figure 6). In addition, the permanent strain rates within the block show an insignificant internal strain rate of less than 0.10 μstrain/yr (Figure 6). Therefore the outer range in the transition zone from the waning collision zone to the Okinawa back arc area appears to act as a quasirigid block. The GPS-derived clockwise rotation rate of 5.1° ± 1.6°/Myr is also in general agreement with those estimated from paleomagnetic and geologic studies, showing a 20° rotation since probably Pliocene (5.6–10.0°/Myr) [*Angelier et al.*, 1990; *Lee et al.*, 1991]. *Lu and Malavieille* [1994] have indicated that the whole outer range (the TAIK and NHSS blocks) acts as a right-lateral shear zone (Figures 1 and 9), based on limited outcrop observations along the coast line; however, because of a very small internal strain observed within the outer range (Figure 6), we propose that the left-lateral motion on the Chinshan–Shanchiao fault system in the frontal area plays a key role as the block-bounding fault results in a quasirigid clockwise block rotation for the outer range (Figure 9) instead of a right-lateral shear zone.

[27] Second, for the RYUK block of the inner range in the transition zone, the best fitting Euler pole is located south of the GPS array within the block (24.341°N and 121.609°E) with an clockwise rotation rate of 47.3° ± 7.8°/Myr (Figure 6). However, the significant internal NW–SE extension at a rate of 0.62 ± 0.09 μstrain/yr exists within this block (Figure 6), implying a ''rigid block'' rotation is not appropriate. Because the estimated Euler pole is located near the collision point between the Luzon arc (the indenter) and the Taiwan mountain belt (Figure 6), we conclude that the deformation in this region is mainly influenced by NW to NNW collision of the Luzon island arc which causes the block rotation at the corner of the converging plates (Figure 9). The dramatic turn of the GPS displacements in the eastern part of this region is similar, to some extent, to that in eastern and southeastern Tibet [e.g., *Thatcher*, 2007] where large rotations are taking place in the eastern corner of the N–S intrusion of the Indian plate. In addition, the velocity field in the northern part of the RYUK block also displays a significant increase of especially southward movement, from west to east toward the Okinawa trough (Figure 3). As a result, we suggest that this represents the influence of a southward opening of the Okinawa trough which was previously interpreted as a result of the Ryukyu Trench retreat offshore in eastern Taiwan. Furthermore, like the model suggested by *Wallace et al.* [2005], as the buoyant Chinese continental crust enters the Luzon arc–Ryukyu subduction system, convergence between the Eurasian plate and the Philippine Sea plate is inhibited (Figure 9). Northwest motion of the Luzon arc coupled with a trench-ward motion of the Okinawa trough is producing rapid block rotation of the RYUK block [*Wallace et al.*, 2005] which is, however, far from rigid (Figure 9).

7. Conclusions

[28] Crustal deformation yielded from the densely spaced decadal GPS measurements (1995–2005) in northern Taiwan shows the transition of surface strain in the type of tectonic activity from an arc–continent collision to a subduction/back-arc opening along the Chinese continental margin. The horizontal velocities with respect to the Chinese margin station, S01R, reveal distinct deformations in three different geological/tectonic areas: (1) a waning collision area, (2) an outer range of the transition zone, and (3) an inner range of the transition zone. It appears that the NW-trending boundary of the subducting Philippine Sea plate across northern Taiwan plays an important role in separating the waning collision area to the west and the transition zone to the east. In the waning collision area, velocities are 0.3–7.3 mm/yr toward the NW. The tectonic blocks within the area represent a significant NW–SE internal contraction rate of ~0.44 μstrain/yr with negligible block rotation (<3.0°/Myr). In the outer range of the transition zone, horizontal velocities of 1.0–7.8 mm/yr from south to north rotate clockwise from 008° to 143°. The tectonic blocks here show a low permanent strain rate of <0.10 μstrain/yr. The location of the Euler pole is near the northeastern tip of the Ilan plain with an angular velocity of 5.1° ± 1.6°/Myr, which is in general agreement with those estimated from paleomagnetic and geologic studies. The Chinshan–Shanchiao fault, which represents the block-bounding fault in the north of this region, is characterized by a left-lateral strike–slip movement with normal motion. In the inner range of transition zone, an even more clockwise rotation from west to east with vectors of 9.3–41.2 mm/yr from 053° to 146° occur here. The tectonic blocks reveal a remarkable NW–SE internal extension rate of ~0.62 μstrain/yr. A notable clockwise rotation rate of ~47.3°/Myr is presented with the Euler pole located south of the GPS array close to collision corner. The Choushui fault is a significant block-bounding fault to the north of this area, which is characterized by a significant oblique normal fault motion with a left-lateral strike–slip component near the central axis of the Ilan plain. We suggest that, in addition to the arc–continent collision-induced rotation, trench roll-back and back-arc opening likely act together in complex ways in this region.

[29] **Acknowledgments.** We thank the Ministry of the Interior (MOI) of Taiwan for the campaign-surveyed GPS data and MOI, IESAS, NCKU, and IGS for continuous GPS data. We are grateful to Associate Editor Timothy Dixon and two reviewers, Rob McCaffrey and David Wiltschko, for the critical comments. This research was partially supported by Taiwan NSC grant 96-2116-M-006-011. Figures were generated using the generic mapping tools (GMT) developed by *Wessel and Smith* [1991].

References

Altamimi, Z., P. Sillard, and C. Boucher (2002), ITRF2000: A new release of the International Terrestrial Reference Frame for earth science applications, *J. Geophys. Res.*, *107*(B10), 2214, doi:10.1029/2001JB000561.

Angelier, J., E. Barrier, and H. T. Chu (1986), Paleostress trajectories related to plate collision in the Foothills fold-thrust belt of Taiwan, *Tectonophysics*, *125*, 161–178.

Angelier, J., F. Bergerat, H. T. Chu, and T. Q. Lee (1990), Tectonic analysis and the evolution of a curved collision belt: The Hsuehshan Range, northern Taiwan, *Tectonophysics*, *183*, 77–96.

Chan, Y. C., K. J. Chang, R. F. Chen, J. C. Lee, and Y. C. Hsieh (2006), Active extensional structures discovered by the Airborne LiDAR mapping in the Tatun volcanic region, Taiwan, *Eos Trans. AGU*, *87*(52), Fall Meet. Suppl., Abstract T33D-0541.

Chen, H. Y., L. C. Kuo, and S. B. Yu (2002), Coseismic movement and seismic ground motion associated with the 31 March 2002 Hualien "331" earthquake, *Terr. Atmos. Ocean. Sci.*, *15*, 683–695.

Chu, C. J., C. T. Lee, and L. S. Teng (1998), Structural features and Quaternary tectonics of the Chinshan fault, northern Taiwan, *J. Geol. Soc. China*, *41*, 25–42.

Clift, P. D., H. Schouten, and A. E. Draut (2003), A general model of arc–continent collision and subduction polarity reversal from Taiwan and the Irish Caledonides, in *Intra-Oceanic Subduction Systems: Tectonic and Magmatic Processes*, *Spec. Publ., Geol. Soc. London*, vol. 219, edited by R. D. Larter and P. T. Leat, pp. 81–98, The Geological Society of London, London, UK.

Goldberg, D. E. (1989), *Genetic Algorithms in Search, Optimization and Machine Learning*, 412 pp., Addison Wesley, Reading, Mass.

Ho, C.-S. (1988), *An Introduction to the Geology of Taiwan: Explanatory Text of the Geologic Map of Taiwan*, 2nd ed., 192 pp., Min. of Econ. Aff., Taipei, Taiwan.

Hsiao, L. Y., K. A. Lin, S. T. Huang, and L. S. Teng (1999), Structural characteristics of the southern Taiwan-Sinzi folded zone, *Petrol. Geol. Taiwan*, *32*, 133–153.

Hu, J. C., J. Angelier, J. C. Lee, H. T. Chu, and D. Byrne (1996), Kinematics of convergence, deformation and stress distribution in the Taiwan collision area: 2-D finite-element numerical modeling, *Tectonophysics*, *255*, 243–268.

Hu, J. C., S. B. Yu, H. T. Chu, and J. Angelier (2002), Transition tectonics of northern Taiwan induced by convergence and trench retreat, in *Geology and Geophysics of an Arc–Continent Collision, Taiwan*, *Geol. Soc. Am. Spec. Pap.*, vol. 358, edited by T. B. Byrne and C. S. Liu, pp. 147–160, The Geological Society of America, USA.

Huang, C. Y., P. B. Yuan, and S. J. Tsao (2006), Temporal and spatial records of active arc–continent collision in Taiwan: A synthesis, *Geol. Soc. Am. Bull.*, *118*, 274–288, doi:10.1130/B25527.1.

Huang, S. Y., C. M. Rubin, Y. G. Chen, and H. C. Liu (2007), Prehistoric earthquakes along the Shanchiao fault, Taipei Basin, northern Taiwan, *J. Asian Earth Sci.*, *31*, 265–276, doi:10.1016/j.jseaes.2006.07.025.

Hugentobler, U., S. Schaer, and P. Fridez (Eds.) (2001), *Bernese GPS Software Version 4.2*, 515 pp., Astronomical Institute, University of Berne, Switzerland.

Jiang, S. C. (1976), Seismic exploration in the Ilan plain, (in Chinese), *Min. Tech.*, *14*, 215–221.

Kao, H., S. J. Shen, and K. F. Ma (1998), Transition from oblique subduction to collision: Earthquakes in the southernmost Ryukyu arc–Taiwan region, *J. Geophys. Res.*, *103*, 7211–7230.

Lee, C. T. (1991), Observation of normal fault system in Toucheng-Chiaohsi area, northeastern Taiwan, in *Proc. 3rd Taiwan Symposium on Geophysics*, pp. 496–508, Chinese Geophysical Society, Chungli, Taiwan.

Lee, C. T., and Y. Wang (1988), Quaternary stress changes in northern Taiwan and their tectonic implication, *Proc. Geol. Soc. China*, *31*, 154–168.

Lee, T. Q., J. Angelier, H. T. Chu, and F. Bergerat (1991), Rotations in the northeastern collision belt of Taiwan: Preliminary results from paleomagnetism, *Tectonophysics*, *199*, 109–120.

Lin, A. T., A. B. Watts, and S. P. Hesselbo (2003), Cenozoic stratigraphy and subsidence history of the South China Sea margin in the Taiwan region, *Basin Res.*, *15*, 453–478.

Lu, C. Y., and J. Malavieille (1994), Oblique convergence, indentation and rotation tectonics in the Taiwan Mountain Belt: Insights from experimental modeling, *Earth Planet. Sci. Lett.*, *121*, 477–494.

Lu, C. Y., J. Angelier, H. T. Chu, and J. C. Lee (1995), Contractional, transcurrent, rotational and extensional tectonics: Examples from northern Taiwan, *Tectonophysics*, *246*, 129–146.

Lu, C. Y., F.-S. Jeng, K.-J. Chang, and W.-T. Jian (1998), Impact of basement high on the structure and kinematics of western Taiwan thrust wedge: Insights from sandbox models, *Terr. Atmos. Ocean. Sci.*, *9*, 533–550.

Lue, Y. T., T. Q. Lee, and Y. Wang (1995), Paleomagnetic study on the collision-related bending of the fold-thrust belt, northern Taiwan, *J. Geol. Soc. China*, *38*, 215–227.

McCaffrey, R. (2002), Crustal block rotations and plate coupling, in *Plate Boundary Zones*, *Geodyn. Ser.*, vol. 30, edited by S. Stein and J. Freymueller, pp. 101–122, AGU, Washington, D. C.

McCaffrey, R. (2005), Block kinematics of the Pacific-North America plate boundary in the southwestern United States from inversion of GPS, seismological, and geologic data, *J. Geophys. Res.*, *110*, B07401, doi:10.1029/2004JB003307.

Okada, Y. (1985), Surface deformation to shear and tensile faults in a halfspace, *Bull. Seismol. Soc. Am.*, *75*, 1135–1154.

Press, W. H., B. P. Flannery, S. A. Teukolsky, and W. T. Vetterling (1989), *Numerical Recipes*, Cambridge Univ. Press, Cambridge, U. K.

Savage, J. C. (1983), A dislocation model of strain accumulation and release at a subduction zone, *J. Geophys. Res.*, *88*, 4984–4996.

Shyu, J. B., K. Sieh, Y. G. Chen, and C. S. Liu (2005), Neotectonic architecture of Taiwan and its implications for future large earthquakes, *J. Geophys. Res.*, *110*, B08402, doi:10.1029/2004JB003251.

Suppe, J. (1984), Kinematics of arc–continent collision, flipping of subduction and back-arc spreading near Taiwan, *Mem. Geol. Soc. China*, *6*, 21–33.

Teng, L. S. (1996), Extensional collapse of the northern Taiwan mountain belt, *Geology*, *24*, 949–952.

Teng, L. S., and C. T. Lee (1996), Geomechanical appraisal of seismogenic faults in northeast Taiwan, *J. Geol. Soc. China*, *39*, 125–142.

Teng, L. S., C. H. Chen, W. S. Wang, T. K. Liu, W. S. Juang, and J. C. Chen (1992), Plate kinematic model for late Cenozoic arc magmatism in northern Taiwan, *J. Geol. Soc. China*, *35*, 1–18.

Teng, L. S., C. T. Lee, C. H. Peng, W. F. Chen, and C. J. Chu (2001), Origin and geological evolution of the Taipei basin, northeast Taiwan, *W. Pacific Earth Sci.*, *1*, 115–142.

Thatcher, W. (2007), Microplate model for the present-day deformation of Tibet, *J. Geophys. Res.*, *112*, B01401, doi:10.1029/2005JB004244.

Thomas, A. L. (1993), Poly3D: A three-dimensional, polygonal element, displacement discontinuity boundary element computer program with applications to fractures, faults, and cavities in the Earth's crust, unpublished M.Sc. thesis, 52 pp., Geology Department, Stanford Univ., California, USA.

Viallon, C., P. Huchon, and E. Barrier (1986), Opening of the Okinawa basin and collision in Taiwan: A retreating trench model with lateral anchoring, *Earth Planet. Sci. Lett.*, *80*, 145–155.

Wallace, L. M., R. McCaffrey, J. Beavan, and S. Ellis (2005), Rapid microplate rotations and backarc rifting at the transition between collision and subduction, *Geology*, *33*, 857–860.

Wang, C. Y., W. C. Hsiao, and C. T. Sun (1994), Reflection seismic stratigraphy in Taipei basin (I)–northwestern Taipei basin, *J. Geol. Soc. China*, *37*, 69–95.

Wang, C. Y., Y. L. Tsai, and M. L. Ger (1995), Reflection seismic stratigraphy in Taipei basin (II)–southwestern Taipei basin, *J. Geol. Soc. China*, *38*, 141–172.

Wells, D. L., and K. J. Coppersmith (1994), New empirical relationships among magnitude, rupture length, rupture width, rupture area, and surface displacement, *Bull. Seismol. Soc. Am.*, *84*, 974–1002.

Wessel, P., and W. Smith (1991), Free software helps map and display data, *Eos Trans. AGU*, *72*(41), 441.

K.-E. Ching and R.-J. Rau, Department of Earth Sciences, National Cheng Kung University, 1 University Road, Tainan 701, Taiwan. (raurj@mail.ncku.edu.tw)

J.-C. Hu, Department of Geosciences, National Taiwan University, No. 1, Sec. 4, Roosevelt Road, Taipei 106, Taiwan.

J.-C. Lee, Institute of Earth Sciences, Academia Sinica, 128 Academia Road Sec. 2, Nankang, Taipei 115, Taiwan.